 http://dx.doi.org/10.7494/mech.2012.31.4.133

Mariusz Biegaj *, **, Kajetan Dziedziech *, **, Adam Macheta *

WORM GEAR ANALYSIS IN TERMS OF NUMERICAL MODELLING

SUMMARY

A worm gear mechanism, widely used in numerous mechanical applications, is the essential component in energy efficiency considerations. Compared to traditional gearboxes, worm gear is characterized by lower value of efficiency, provided by the manufacturers as 70–90%. However, the efficiency level can differ depending on the specific conditions of operation such as output torque, input rotational velocity, ambient temperature and type of lubrication. In order to analyse and simulate the worm gear mechanism in mechanical systems, it is essential to establish the actual efficiency value for specific conditions. The following article contains the description of efficiency test performed for the worm gear as a part of tram pantograph system studied in frame of ESTOMAD project. The aim of the experiment was to determine the actual efficiency value of the transmission tested. The worm gear has been tested in an open loop configuration, therefore the efficiency has been determined basing on input and output torque and rotational velocity measurements. The tests have been performed for various output torques and input velocities to obtain view on losses in worm gear under different operational conditions, paying special attention to the velocity that drives the pantograph mechanism. The efficiency changes with the output torque variation, while the impact of rotational velocity level on the mentioned value is minimal. The results of measurements are used in modelling phase of worm gear component in 1D simulation environment, particularly creating new model and its correlation and validation.

***Keywords**: worm gear, pantograph mechanism, efficiency, open loop configuration, 1D model*

ANALIZA SPRAWNOŚCI PRZEKŁADNI ŚLIMAKOWEJ NORD FLEXBLOC SK 1SI63

Mechanizm przekładni ślimakowej, szeroko stosowany w wielu urządzeniach mechanicznych, jest elementem charakteryzującym się niską sprawnością, co nie jest dobrze postrzegane z energetycznego punktu widzenia. W porównaniu z tradycyjnymi przekładniami, przekładnia ślimakowa charakteryzuje się niższą wartością sprawności, określanej przez producentów na poziomie 70–90%. Jednakże poziom sprawności takiej przekładni może zmieniać się w zależności od warunków pracy, takich jak obciążenie, wejściowa prędkość obrotowa, temperatura otoczenia oraz sposób smarowania. W celu analizy i symulacji działania przekładni ślimakowej stosowanej w konkretnym systemie mechanicznym, ważne jest, aby określić właściwy poziom sprawności w określonych warunkach pracy układu. Artykuł ten przedstawia badania sprawności przekładni ślimakowej, będącej częścią pantografu tramwajowego analizowanego w ramach projektu ESTOMAD. Celem eksperymentu było określenie rzeczywistej wartości sprawności badanej przekładni. Przekładnia ślimakowa została poddana testom na stanowisku zbudowanym w postaci otwartego łańcucha kinematycznego, dlatego też sprawność została określona na podstawie pomiarów momentu oraz prędkości obrotowej na wejściu i wyjściu przekładni. Testy były przeprowadzone dla różnych obciążeń i prędkości obrotowych, aby oszacować straty w urządzeniu w zróżnicowanych warunkach eksploatacyjnych, w szczególności biorąc pod uwagę prędkości obrotowe stosowane w przypadku mechanizmu podnoszenia pantografu. Sprawność przekładni zmienia się wraz ze zmianą momentu obciążającego, natomiast wpływ zmian prędkości obrotowej na sprawność był bardzo niewielki. Wyniki pomiarów są wykorzystane w procesie modelowania przekładni w środowisku symulacyjnym 1D, podczas tworzenia nowego modelu oraz jego korelacji i walidacji.

***Słowa kluczowe**: przekładnia ślimakowa, pantograf, sprawność, konfiguracja „open loop”, model 1D*

1. INTRODUCTION

The aim of the experiments presented in the following article was to determine the losses in the worm gear for different operating conditions such as torque on the output and the influence of rotational velocity on the input of transmission. The worm gear is a part of the tram pantograph system analysed in frame of the ESTOMAD project in the context of overall efficiency of the mechanism. Worm gear is a part of pantograph drive subsystem along with a DC motor and a lead screw. The input torque is provided to the worm by the electric motor, while the worm wheel shaft is connected to the lead screw. The complete drive ensures the up and down motion of pantograph mechanism to connect the tram with electric line. Worm gear was identified as an element contributing to the greatest extent of losses in the drive. Losses in transmission are the cause of elevated temperature and significant load of the electric motor, which could lead to damage and disable the drive in long term tests. Therefore, a detailed study of mechanism efficiency was necessary.

* EC Engineering Sp. z o. o., Kraków
** AGH University of Science and Technology, Krakow, Poland

The transmission tests have determined the overall efficiency level of the device for different values of output torque and input rotational velocity. Additional motivation to conduct this type of experiment was to create a numerical model of the worm gear in order to perform the simulations of this component in 1D environment. In this case it was necessary to determine the level of different types of losses, both in tooth engagement of worm and worm wheel, as well as resulting from the shafts bearing and oil churning and build proper mathematical model of these losses.

2. LABORATORY TEST OF WORM GEAR

This chapter is devoted to laboratory tests of worm gear. In first subchapter object of tests, namely gearbox NORD FLEXBLOC SK 1SI63 is presented with its technical data (Flexbloc & Minicase Worm Drivers). Second subchapter describes test rig that has been used for determination of energetic parameters of investigated object. Another subchapter briefly describes scope of measurements, which have been conducted. Last subchapter presents obtained results along with simple conclusions.

2.1. Technical specification

The worm gear analysed in frame of the article is a typical transmission consisted of worm and worm wheel. The particular tested gearbox is shown in the Figure 1.

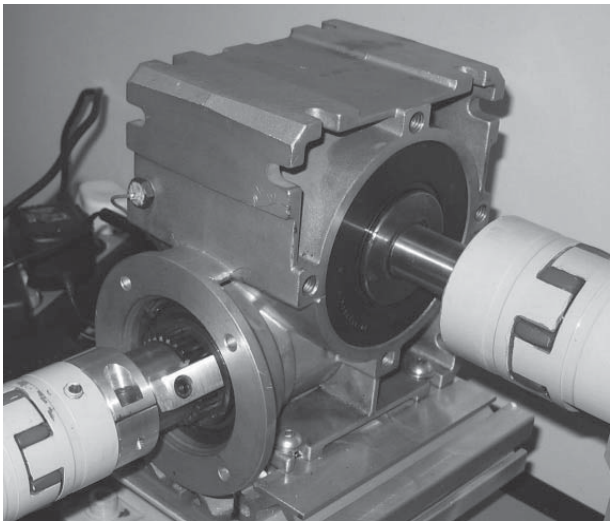

Fig. 1. Object of testing

A short technical specification has been presented in Table 1. Despite the fact that efficiency value has been provided, it was necessary to determine the actual efficiency levels for specific working conditions of variable torque, rotational velocity and lubrication.

Table 1

Essential parameters of tested worm gear

Parameter	Value
Nominal efficiency (at n_1 = 1400 min^{-1})	89%
Start-up efficiency	67%
Gear ratio	7.5
Worm wheel diameter	90 mm
Worm diameter	63 mm
Normal pressure angle	20°
Lubricant	CLP PG 220 (Alphasyn GS 220)

The analysis of device required thorough knowledge about geometrical parameters describing the engagement between worm and worm wheel. Basic geometrical parameters used for calculations have been summarized in Table 2.

Table 2

Basic geometrical parameters

Parameter	Worm	Worm wheel
Teeth number [mm]	4	30
Measured diameter [mm]	42.2	97.7
Width [mm]	39.4	25
Gear ratio	7.5	

The quantities crucial for further investigation have been calculated based on parameters from Table 2 and presented in Table 3.

Table 3

Calculated geometrical parameters

Parameter	Worm	Worm wheel
Lead angle λ [°]	18.92	71.08
Helix angle ψ [°]	71.08	18.92
Apparent friction angle Φn [°]	6.73	19
Pitch diameter d [mm]	35	90

Shaft's bearing, as a component contributing to the overall losses, has been realized with use of standard ball bearing codenamed as shown in Table 4.

Table 4

Ball bearings models used in analysed gearbox

Bearing model	
6211 C 43,0 (worm wheel shaft)	2 pcs (worm wheel shaft)
6009 2Z C3	1 pc (worm shaft)
6202	1 pc (worm shaft)

Gearbox lubrication is ensured by the oil circulating in the housing in the amount of 180 ml. Parameters of used lubricant are quite important in terms of energy loss. The manufacturer provides a worm gear with Alphasyn GS 220 (CLP PG type) oil with parameters summarized in Table 5 (Datasheet of GS 220 oil). The analysis of losses requires the knowledge about the oil viscosity characteristic in a range of operating temperature. The investigation is presented in the further chapters of the following paper.

Table 5

Specification of CLP PG 220 oil type

Parameter	Value
Density	1 g/ml
Kinematic viscosity (at 40°C)	220 cSt
Kinematic viscosity (at 100°C)	36 cSt

2.2. Measurement setup

The entire experimental campaign was performed in an open loop configuration test rig. In such configuration the energy is transferred from the electric motor to the powder brake through the worm gear and the system of couplings. Within the test the following quantities have been acquired: rotational velocity on the input shaft (obtained directly from the VFD controller), torque on the input and output shaft, oil temperature in the worm gear housing. Rotational velocity on the output shaft has been calculated based on the gear ratio. The diagram of the test rig is shown in the Figure 2.

The test rig has been driven with a 4kW three-phase induction motor with rated speed of 2815 rpm, manufactured by TAMEL. The motor has been controlled with LG iS5 frequency converter (inverter). The inverter allows scalar control with U/f linear characteristic and what is more sensor and sensorless vector control of torque or rotational velocity. During the tests, the inverter was working in vector control mode, which ensured the operation with the rotational velocity on the established level. The tested worm gear has been loaded with powder brake with power dissipation of 2 kW, manufactured by EMA-ELFA, type P170HV. The brake ensures the 5% accuracy maintaining the value of torque in the whole range of rotational velocity. The brake's output torque is independent of slip speed and working temperature. MECMESIN torque sensors have been installed on the input and output of worm gear. The signals from torque sensors and the rotational velocity have been acquired with SPIDER-8 measurement system manufactured by HOTTINGER. Temperature measurement is based on the resistance temperature detector PT100 installed in the worm gear housing. The resistance of the detector has been measured with METEX multimeter. The connections of all shafts of drive and load systems of test rig have been executed with torsionally flexible couplings, ROTEX (KTR) type. The drive from the motor to the gearbox input shaft is transmitted via a toothed belt. In order to decrease the influence of external conditions the ambient temperature has been as stable as possible during the tests (22°C). The test rig described in the paper has been built specially for this particular worm gear tests. The complete setup, except data acquisition instruments is shown in Figure 3.

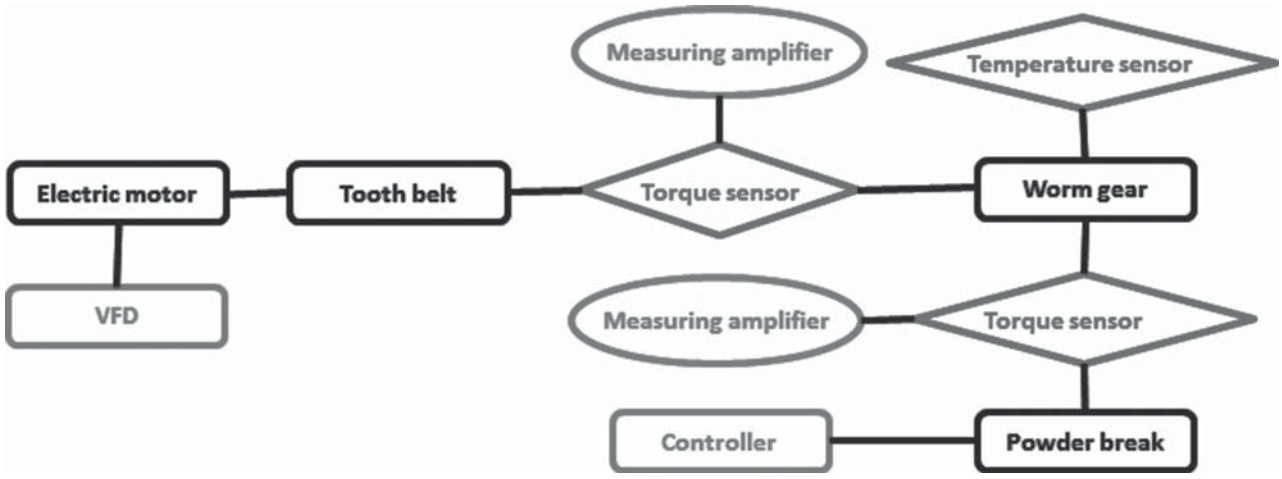

Fig. 2. Test rig configuration

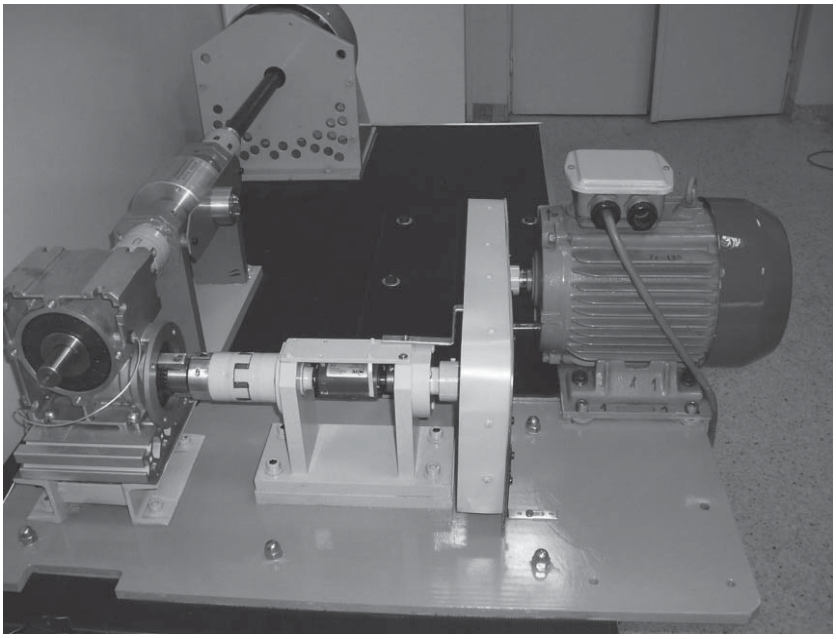

Fig. 3. General view of test rig used in the experiments

2.3. Test plan

Tests have been performed for various operational conditions in order to provide the essential information concerning efficiency characteristic of analysed transmission. The test cases have been summarized in Table 6.

The efficiency has been determined based on the output to the input power ratio calculated with use of input and output torque and input velocity data.

Along with torque and rotational velocity, the temperature of oil has been acquired during every individual test in order to investigate the influence of the temperature on the overall efficiency of tested transmission.

Large number of test configurations allowed to investigate the influence of individual parameters on the overall worm gear efficiency. Tests performed for constant output torque provided information about the impact of the other parameters (rotational velocity, temperature) on the efficiency value. Analogically, experiment with fixed temperature has been done. The results of tests without torque on the output provided the information about the churning losses characteristic, since bearing and tooth engagement losses are extremely small during the non-load test and have been ignored. Therefore, it was possible to prepare relevant experimental model of churning power losses. Additionally, the experiments with standard and decreased oil level have been executed in order to check the impact of lubrication on the overall energetic behaviour of device.

2.4. Experimental results

The general view on losses during the work in various operational conditions is presented in Figure 4 as efficiency characteristics in function of output torque vs. input rotational velocities.

As mentioned in previous chapter, the tests have been performed for various configurations of operational parameters to obtain good view on losses under different operational conditions. Figure 5 shows the efficiency characteristic as a function of output torque acquired at 1500 and 2000 rpm. During this particular experiment the oil temperature has been stable and equal to 58°C.

Based on the presented results, it can be stated that overall efficiency of the device is mainly load dependant. Increased temperature and therefore lower viscosity of oil contributed to efficiency rise of about 3%. The influence of rotational velocity on the efficiency is also minimal.

Aside from measurements done in working conditions, measurements have been also conducted in idle condition. Results are presented in Figure 6.

Table 6

Test cases used in worm gear experiments

Input rotational velocity [rpm]	Output torque [Nm]	Lubrication
1200, 1500, 2000,2400, 2800	No torque, 5, 15, 25, 30, 40, 50, 60, 70, 80, 90	Standard oil level, decreased oil level

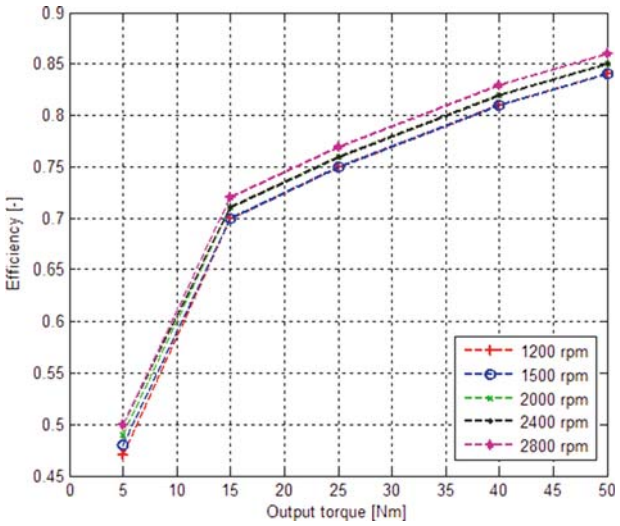

Fig. 4. Efficiency characteristics of tested worm gear

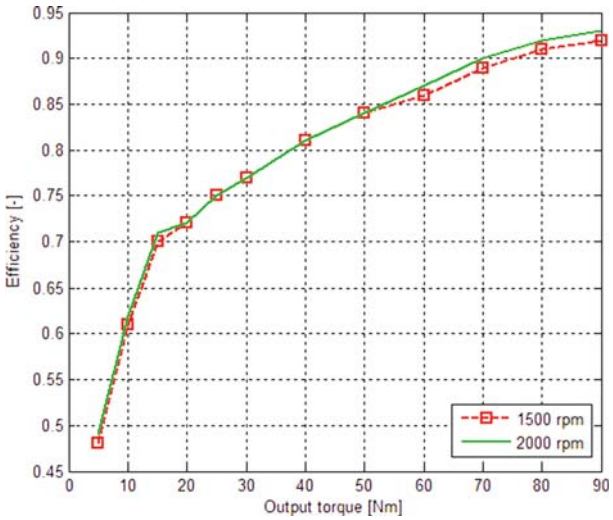

Fig. 5. Efficiency as a function of output torque for 1500 and 2000 rpm (at constant temperature = 58°C)

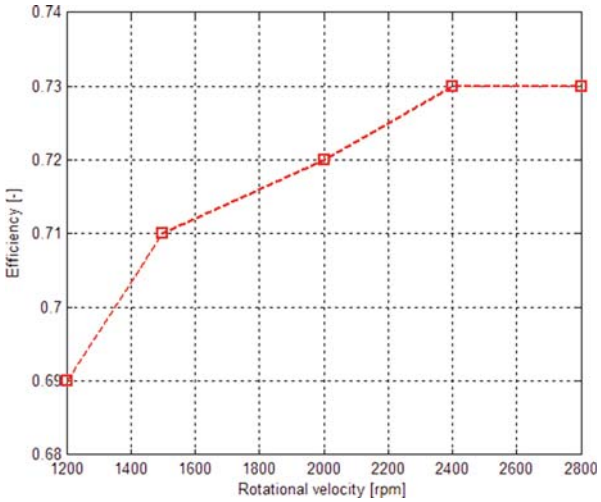

Figure 6. Efficiency as a function of rotational velocity (idle condition)

3. MATHEMATICAL MODEL OF THE ENERGY LOSS

This chapter is devoted to mathematical modelling of worm gear along with model building, correlation and validation process. At the beginning considerations concerning origin of losses are presented. Another three subchapters presents mathematical models for particular type of losses investigated. In case of tooth engagement losses and churning losses, basic formulas are given. As for bearing losses, they are presented with geometrical constrains. Gearbox geometry has been measured and presented in subchapter 3.4. This geometry has been used for determination of forces on particular bearings. Thanks to well established mathematical models of bearings power losses as a function of force it was possible to determine, bearing power losses as a function of input torque and friction coefficient. Last two subchapters considered mathematical model correlation and validation.

3.1. Origin of losses

Understanding the origin of losses is very important aspect of efficiency optimizing process. Having this knowledge one can determine influence of operating parameters on total losses of the system and indicate most important source of those losses. Losses in worm gear can be divided into three main types: tooth engagement losses, oil churning losses and bearing losses. The overall power loss is equal to the sum of mentioned components. The analysis of mathematical models available in the literature along with experiments performed, results in creation of complete model of overall power loss in the worm gear, ready to be implemented to the 1D simulation environment.

3.2. Losses due to tooth engagement

The literature provide relevant model of tooth engagement losses in the transmission (Gopinath and Mayuram). These losses are represented by the equation:

$$L_t = 2,3\left(\frac{1}{Z_1}+\frac{1}{Z_2}\right)W \tag{1}$$

where:

L_t – tooth engagement power losses [kW]
μ – coefficient of friction between the teeth [–]
Z_1, Z_2 – numbers of teeth on worm and gear [–]
W – total power transmitted [kW]

3.3. Churning losses

Churning losses model have been built as an empirical model with use of data obtained during zero torque measurements. The model is mainly based on the empirical models from available literature, as there is no well-established mathematical model for churning losses, just general formula has been used, and coefficients have been assumed to be unknown and to be correlated (Stavytskyy et al. 2010). Proper model of churning losses require the knowledge about the oil viscosity characteristic. Viscosity of oil is temperature dependent and with growing temperature viscosity decreases according to Arrhenius model (Connors 1990). Kinematic viscosity chaaracteristic can be determined with the following equation:

$$\mu = \mu_0 \cdot e^{-bT} \tag{2}$$

where:

T – operating temperature
μ_0 – linear coefficient
b – exponential coefficient

The values of coefficients μ_0 and b have been obtained with use of two kinematic viscosity values for fixed temperatures presented in previous chapters (Table 5). The characteristic of oil viscosity has been plotted and shown in Figure 7. Please note that Y axis is expressed in logarithmic scale.

For churning losses determination it was assumed that churning losses (L_{CH}) are non-load-dependent while bearing losses (L_B) and tooth engagement losses (L_T) are load dependent. Therefore, measurement data used in churning losses modelling has been acquired with no load on the output shaft of the worm gear. Basing on the initial assumptions, it can be stated that $L_B = 0$ and $L_T = 0$. As a result, churning loss value is equal to the overall loss. Subsequently, power loss and viscosity values have been calculated with use of measurement data. Finally, the complete empirical model of churning losses as a function of rotational velocity and oil temperature has been built

$$L_{CH} = \mu(T)(\alpha \cdot \omega^{\beta} + C) \tag{3}$$

where:

α – linear coefficient
β – exponential coefficient
C – constant
ω – rotational velocity

3.4. Losses due to friction in bearings

Bearing losses consideration required the knowledge about the forces distribution present in every bearing in the worm gear. First step was to analyse the forces acting in the worm and the gear. The forces acting on the worm are distributed as shown in Figure 8. The forces acting on worm wheel are analogical to the forces on worm.

The forces acting in gear's contact point can be transmitted to the forces in bearings (C and D) with use of torque equations about selected axis and through selected points. The schematic drawing shown on Figure 9 shows forces distribution and crucial distances used for equations building.

Analogical approach has been adapted to worm wheel shaft analysis. Similar schematic drawing has been prepared as shown in Figure 10.

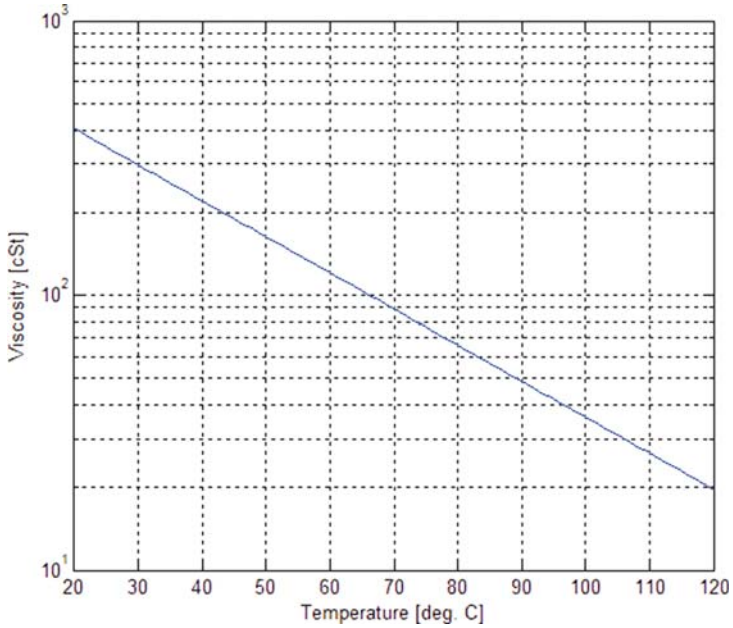

Fig. 7. Viscosity of oil characteristic in range of temperature

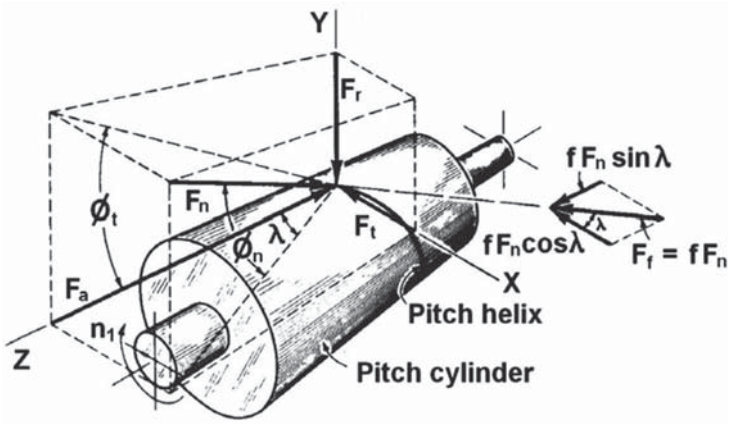

Fig. 8. Forces distribution on the worm

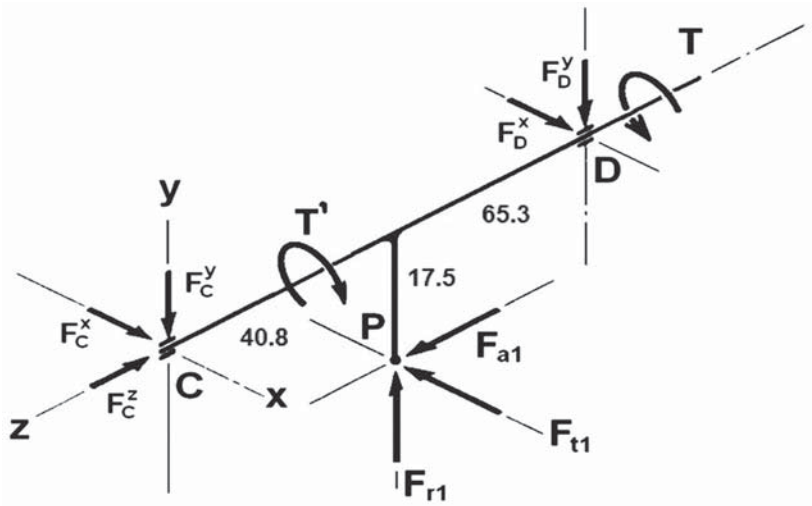

Fig. 9. Forces distribution on the worm shaft

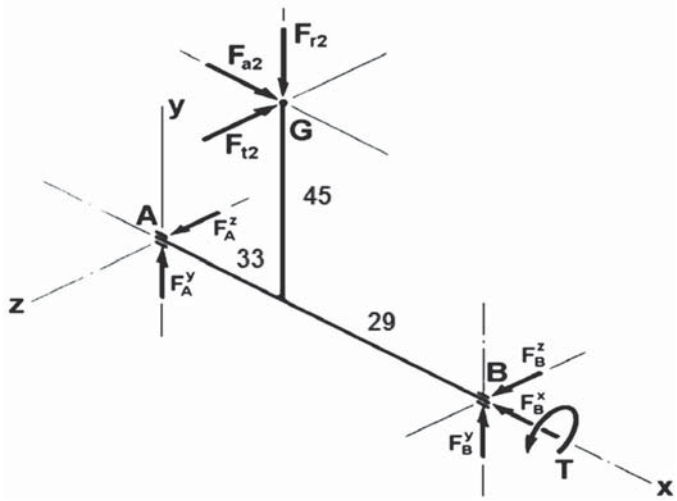

Fig. 10. Forces distribution on worm wheel shaft

Based on the above diagrams, the resultant forces acting in every bearing in worm gear have been obtained as functions of input torque and friction coefficient between worm and worm wheel.

Total forces acting in every bearing are the input to the mathematical model of power losses. In the analysis presented in this paper, SKF model has been used (SKF Bearing Calculator).

$$F_A = \sqrt{(F_A^y)^2 + (F_A^z)^2} = \sqrt{\left(\frac{0.0548}{0.00564 + 0.0166 \cdot \mu} - 41.45) \cdot T\right)^2 + \left(\frac{0.468 \cdot T \cdot (0.939 - 0.324 \cdot \mu)}{0.00564 + 0.0166 \cdot \mu}\right)^2} \tag{4}$$

$$F_B = \sqrt{(F_B^y)^2 + (F_B^z)^2} = \sqrt{\left(T \cdot \left(\frac{0.0622}{0.00564 + 0.0166 \cdot \mu} + 41.45\right)\right)^2 + \left(\frac{0.532 \cdot T \cdot (0.939 - 0.324 \cdot \mu)}{0.00564 + 0.0166 \cdot \mu}\right)^2} \tag{5}$$

$$F_C = \sqrt{(F_C^x)^2 + (F_C^y)^2} = \sqrt{(35.169 \cdot T)^2 + \left(\frac{T \cdot (0.024 - 0.00567 \cdot \mu)}{0.000598 + 0.00176 \cdot \mu}\right)^2} \tag{6}$$

$$F_D = \sqrt{(F_D^x)^2 + (F_D^y)^2} = \sqrt{(21.947 \cdot T)^2 + \left(\frac{0.117 \cdot T}{0.00564 + 0.0166 \cdot \mu} - \frac{T \cdot (0.024 - 0.00567 \cdot \mu)}{0.000598 + 0.00176 \cdot \mu}\right)^2} \tag{7}$$

3.5. Model correlation

The main goal of correlation process was to establish the values of coefficients and constant present in equation 3 for calculation of churning losses and then friction coefficient for calculation of tooth engagement losses. Since simultaneous correlation is very difficult, it was decided to conduct entire correlation process in two steps. As it was already mentioned in paragraph 3.3 churning losses are assumed not to be load dependant and therefor the values of coefficients and constant present in equation 3 will be determined in idle conditions. In order to achieve satisfactory results an average of 5 measurement runs with different rotational velocity were taken and the sum of errors between simulation and measurement results was the minimization criteria. Results of first correlation step are presented in Table 7.

Table 7

Comparison of measured and simulated efficiencies for idle conditions

Rotational velocity [rpm]	Torque [Nm]	
	Measured	Simulated
1200	0.69	0.70
1500	0.71	0.71
2000	0.72	0.72
2400	0.73	0.73
2800	0.73	0.74

Second correlation step concerns tooth engagement and bearing losses as they are coupled by friction coefficient.

Friction coefficient directly influences the bearing load distribution and therefore influences bearing losses. Results of second correlation step are presented in Table 8.

Table 8

Comparison of measured and simulated efficiencies for operational conditions

Torque [Nm]	Efficiency [-]			
	Rotational velocity 1500 [rpm]		Rotational velocity 2000 [rpm]	
	Measured	Simulated	Measured	Simulated
5	0.48	0.45	0.49	0.46
10	0.61	0.62	0.62	0.62
15	0.70	0.70	0.71	0.70
20	0.72	0.74	0.72	0.74
25	0.75	0.76	0.75	0.76
30	0.77	0.78	0.77	0.78
40	0.81	0.80	0.81	0.80
50	0.84	0.84	0.84	0.84
60	0.86	0.87	0.87	0.87
70	0.89	0.90	0.90	0.90
80	0.91	0.91	0.92	0.91
90	0.92	0.93	0.93	0.94

Complete correlated numerical model is able to simulate the overall power loss and therefore the efficiency of analyzed device. The result of simulation of worm gear energetic behavior in 1D environment is shown in Figure 11 as a function of input rotational velocity and output torque.

3.6. Model validation

After obtaining a correlated efficiency map of considered worm gear it is necessary to validate whether the model represents the energetic behaviour of the object precisely enough. Since the correlation process has been conducted using measurement data in idle condition and in some part of operational condition, the validation has been done with the remaining sets of measurement data.

Table 9

Comparison of measured and simulated efficiencies for operational conditions

Torque [Nm]	Efficiency [-]			
	Rotational velocity 1200 [rpm]		Rotational velocity 2400 [rpm]	
	Measured	Simulated	Measured	Simulated
5	0.47	0.44	0.5	0.47
15	0.70	0.70	0.71	0.71
25	0.75	0.76	0.76	0.76
40	0.81	0.80	0.82	0.81
50	0.84	0.84	0.85	0.84

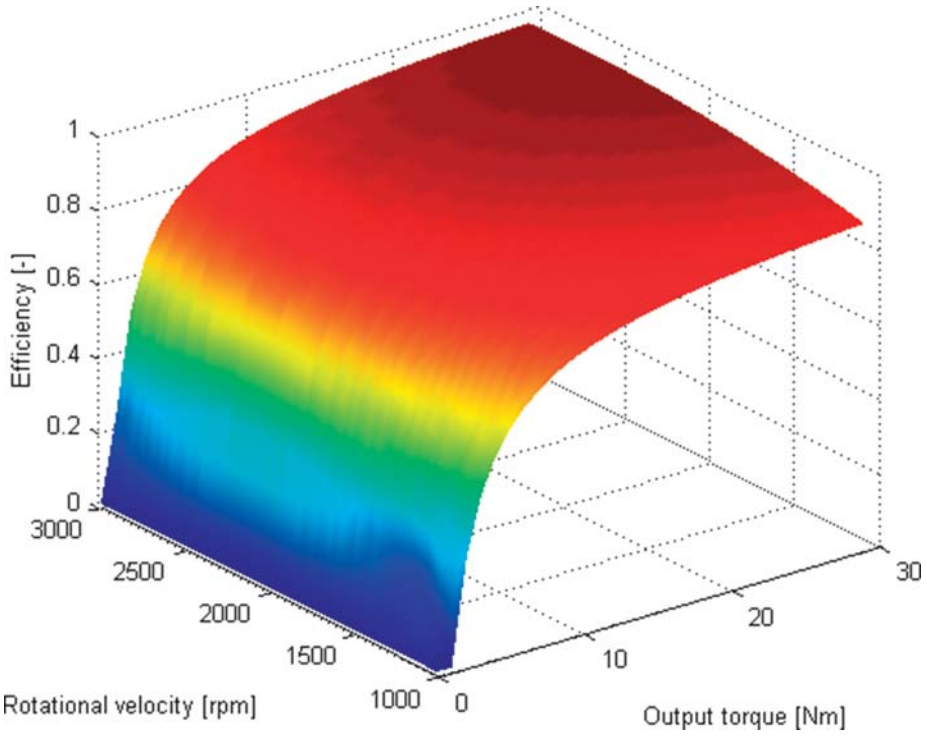

Fig. 11. The efficiency of worm gear as a function of output torque and input rotational velocity

Table 9 shows the correspondence between the simulation of correlated model and the measurements results for efficiency values.

4. CONCLUSIONS

Experiments conducted on the worm gear provided valuable information on its energetic behaviour. The test data obtained from measurements allowed the determination of losses with respect to different operational conditions (torque, rotational velocity, lubrication). The measurements results have shown that the torque is contributing to the worm gear overall efficiency in the greatest way. Other operational parameters influence the losses insignificantly, however they have been take into account as well. As a result of power losses analysis, it was possible to create a proper model that combines an empirical model based on the performed measurements and a mathematical model based on the considerations contained in the available literature. Model implemented into the AMESim environment has shown a good correspondence between simulated and measured total power loss. Maximum observed error value remained under 7%, therefore worm gear efficiency model proved to be reliable and ready to be used in energy flow simulations and considerations. Since the influence of churning losses is not significant the presented model could be used for energetic considerations on different models of worm gears, however if a high precision is required an additional correlation of churning losses equation parameters should be performed.

References

Flexbloc & Minicase Worm Drives, Gear Motors & Speed Reducers. NORD Drivesystems.

Datasheet of GS 220 oil, ARAL, Warszawa, ProduktInfo 2005-07-15/MG.

Gopinath K., Mayuram M. M., *Machine Design II*, Indian Institute of Technology, Madras.

Stavytskyy V., Nosko P., Fil P., Karpov A., Velychko N. 2010, *Lload-independent power losses of gear systems: a review*, TEKA Kom. Mot. i Energ. Roln., t. 10, pp. 205–213.

Connors K. A. 1990, *Chemical Kinetics: The Study of Reaction Rates in Solution*, John Wiley & Sons.

SKF Bearing Calculator. http://webtools3.skf.com/BearingCalc/: SKF.

MECHANICS AND CONTROL
Vol. 31 No. 4 2012 http://dx.doi.org/10.7494/mech.2012.31.4.143

Dariusz Dąbrowski*, Jan Adamczyk*

ANALYSIS OF VIBRATIONS GENERATED BY THE MULTI-BODY MODEL OF A PLANETARY GEAR

SUMMARY

In the paper the dynamic model of an one-stage planetary gear was presented. The model was developed on the basis of a multi-body dynamics method. To conduct dynamic simulations the specialized multi-body dynamics software was used. In the study the tests results for steady state operations of the planetary gear were presented. In the paper the meshing force signals were analyzed. The vibrations generated by the model consist of carrier and gear meshing frequency harmonics. On the spectra the amplitude modulations of the gear meshing frequencies harmonics were observed.

Keywords*: gear model, planetary gear model, multi-body dynamics model, condition monitoring, meshing forces*

ANALIZA SYGNAŁÓW WIBROAKUSTYCZNYCH GENEROWANYCH PRZEZ MODEL PRZEKŁADNI PLANETARNEJ

W artykule został przedstawiony model dynamiczny jednostopniowej przekładni planetarnej. Zbudowano go, korzystając z metody układów wieloczłonowych. W celu przeprowadzenia analiz dynamicznych wykorzystano specjalistyczne oprogramowanie komputerowe. W pracy przedstawiono wyniki symulacji pracy przekładni przy stałej prędkości obrotowej i stałym obciążeniu. Badanymi sygnałami były zmiany wartości sił podczas pracy przekładni, generowane przez algorytm kontaktów między współpracującymi zębami kół zębatych. W wyniku oddziaływań pomiędzy elementami przekładni generowane są sygnały o częstotliwościach związanych z obrotami jarzma oraz pracą zazębienia kół zębatych. W paśmie częstotliwości zazębienia pojawiają się składowe podstawowe oraz ich modulacje.

Słowa kluczowe*: model przekładni, model przekładni planetarnej, metoda układów wieloczłonowych, diagnostyka techniczna, siły zazębienia*

1. INTRODUCTION

In the paper the simulations results for one stage planetary gear model have been presented. The purpose of the analysis was to simulate and verify vibration signals generated by the model of the planetary gear. The multi-body dynamics method has been used to model dynamic interactions occurring during work of the gears.

The dynamic models of the gears developed on the basis of multi-body dynamic method were presented in the papers (Dresig 2005, Kong et al. 2008, Sommer et al. 2011, Wu et al. 2011). In the study (Kong et al. 2008) model of a large industrial gearbox developed in the specialized multi-body dynamics software MSC ADAMS was presented. The authors presented a rigid-elastic model of gears. In this model shafts and gear's bodies are rigid and the contact surfaces between teeth are elastic. The simulation results for other technical states (broken tooth) in this paper were presented. The other model of a spur gears was presented in (Sommer et al. 2011). In this study the multi-body kinematic model of a slider-crank mechanism was presented, the model was developed by a specialized software. In the model authors assume a non-linear contacts between teeth of spur gears. The simulation results were presented for defects of gears such as a chipped and eccentric tooth. The application of the multi-body dynamics method for modeling of a planetary gear dynamics was presented in the articles (Dresig 2005, Wu et al. 2011). In this paper the analyzes of a contact force between a planetary gear teeth in mesh were conducted. The authors noticed that value of analyzed force strongly depend from contact ratio for each gear. The analysis of local faults due to chipped tooth for sun gear were presented, too. With comparison to the perfect geometry a planetary gear with a chipped tooth of the sun gear, in the tests caused large changes of an angular velocity magnitude. The other model presented in the paper (Dresig 2005) permits to conduct the dynamic simulation of planetary gearboxes with arbitrary number of elastically mounted planets, considering the stiffness characteristics in the tooth contacts, as well as all relevant toothing parameters, such as number of teeth, pressure angle, etc.

In the study conducted so far there is no particular analysis of spectrum structure of vibrations generated by the multi-body dynamics models. In the papers (Dresig 2005, Wu et al. 2011) there is no analysis of gear meshing frequencies and its modulations generated by a planetary gear system.

* AGH University of Science and Technology, Department of Mechanics and Vibroacoustics, Krakow, Poland

2. PRELIMINARY MODEL STUDIES

In this chapter the preliminary analyzes of the one-stage planetary gear dynamic model have been presented. In the study the structure containing a sun and planet gear was modeled. In this structure an axis of the planetary gear was constrained, as a result, this model was reduced to a spur gear. Firstly, the three-dimensional CAD model was developed, then it was imported to the MSC ADAMS software. The software allows to conduct dynamic simulations of the model on the basis of a multi-body dynamics method. The model of two gears in mesh is presented in Figure 1.

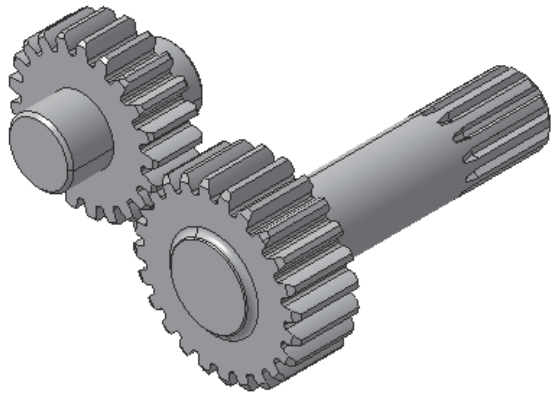

Fig. 1. Model of two gears in mesh

The motion of a multi-body system can be described in general form by the set of equations (1–2) presented below (Wojtyra et al. 2007).

$$G(y, \dot{y}, t) = 0, \qquad y(t = 0) = y_0 \tag{1}$$

$$y = [u^T, p^T, \varepsilon^T, r^T \varphi^T, \lambda^T, F^T, \bar{N}^T]^T \tag{2}$$

Where u is a velocity vector, p is a generalized momentum, ε is an angular velocity, r is a coordinate of the origin of the body reference, φ is an Euler angles, λ is a Lagrange multipliers, F is an external force vector, N is an external torque vector.

For simulation of a vibration signal for gears in mesh the contacts between gears bodies were modeled. In the presented model gears bodies and shafts are rigid, but contact surfaces between gears teeth are elastic. The gears and shaft were fixed, the revolute joints were used between the shafts and ground. The constant rotational motion was applied on the one shaft and resistive torque on the other one. The meshing of the gears was modeled on the basis of contacts, to this aim the ADAMS Impact Algorithm (Kong 2008, MSC Inc. 2011) was used, Figure 2.

Equation (3) describes a contact force in the ADAMS Impact algorithm. The contact force is composed of two parts: the elastic component and damping force, which is a function of the contact-collision velocity. By the definition of the step function equation (4), the damping force is defined as a cubic function of the penetration depth (Sommer 2011, MSC Inc. 2011).

$$F = \begin{cases} K(x_0 - x)^e + CS\dot{x} & x < x_0 \\ 0 & x \geq x_0 \end{cases}. \tag{3}$$

$$S = \begin{cases} 0 & x > x_0 \\ (3 - 2\Delta d)\Delta d^2 & x_0 - d < x < x_0 \\ 1 & x \leq x_0 - d \end{cases} \tag{4}$$

Where $\Delta d = x_0 - x_1$ is a deformation of a body, K is a contact stiffness, e is a force exponent, C is a damping parameter and penetration depth is assigned by d. The stiffness between teeth pair in contact can be described by the Hertz elastic contact theory, equation (5). In this model the stiffness is described by a pair of ideal cylinders in contact (Johnson 1985).

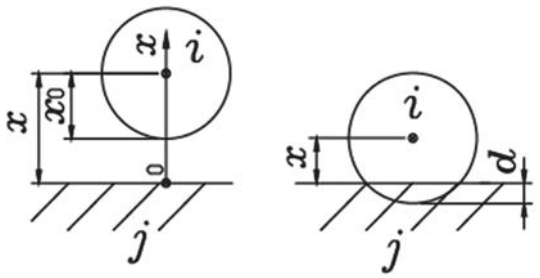

Fig. 2. Contacts model in ADAMS

$$\begin{cases} K = \dfrac{4}{3} R^{\frac{1}{2}} E^* = \dfrac{4}{3}\left[\dfrac{id_1 \cos(\alpha_t)\tan(\alpha'_t)}{2(1+i)\cos(\beta_b)}\right]^{\frac{1}{2}} E^* \\ \dfrac{1}{E^*} = \dfrac{1-\nu_1^2}{E_1} + \dfrac{1-\nu_2^2}{E2} \\ \beta_b = \operatorname{atan}(\tan\beta\cos\alpha_t) \end{cases} \tag{5}$$

In the equation above the R is an equivalent radius of two contacting bodies, E^* is an equivalent Young's modulus of two contacting bodies, i is a gear ratio, d_1 is a diameter of standard pitch circle, α_t', α_t is a transverse pressure angle at engaged and standard pitch circle, β, β_b is a helical angle at the pitch and base circle, ν_1, ν_2 is a Poisson ratio of the pinion and gear. The Young's modulus of pinion and gear are described by E_1, E_2, respectively. In the model it was assumed that the gears are made from the steel with Young modulus $2.1 \cdot 10^{11}$ Pa, and Poisson ratio 0.3. The equivalent Young modulus for two bodies in contact $1.153 \cdot 10^{11}$ Pa. The contact stiffness calculated on the basis on the equation (5) yields to $K = 3 \cdot 10^5$ N/mm$^{3/2}$. The damping coefficient takes value from 0.1 to 1% of K, in the study $C = 3000$ Ns/mm was assumed. Other parameters for con-

tact algorithm: force exponent e = 1.3 and penetration depth d = 0.3mm

The tests results for the multi-body model of gears, were presented below. In the simulation next parameters were assumed: rotational speed 10 Hz, torque 200 Nm, time of simulation 1 s and number of steps 5000. To present the contact force changes in meshing process, the meshing force was plotted in the window (length of 0.06s), and presented in Figure 3.

In Figure 3 the signal of meshing force measured in vertical direction was presented. The signal was calculated on the basis of the contact algorithm between two gears. The presented signal is periodic, changes of signal amplitude are due to number of teeth in engage. The Figure 4 presents spectral analysis of this signal. On the spectrum the Gear Meshing Frequency harmonics (GMF) are clearly distinguishable. According to the equation (6) the GMF should be localized on 240, 480, 700 and 940 Hz.

$$F_m = zF_{rot}n \tag{6}$$

In the equation (6) F_m is a gear meshing frequency, F_{rot} is a rotational frequency, z is a teeth number and n is a number of harmonic.

To sum up, the model of the spur gears allows for simulations of a meshing force in a steady state conditions. The correctness of the results was confirmed by correct localization of GMFs for simplified model.

3. THE PLANETARY GEAR MODEL

The planetary gear model was developed for the planetary gear MERCURY 1-A. In the model all gear dimensions and toothing parameters were reproduced. The planetary gear MERCURY 1-A is a part of the test rig in the Laboratory of Technical Diagnostics at the AGH University of Science and Technology, the test rig was designed for simulation of vibrations generated by the planetary gear under time varying operations. The planetary gear MERCURY 1-A was presented in Figure 5.

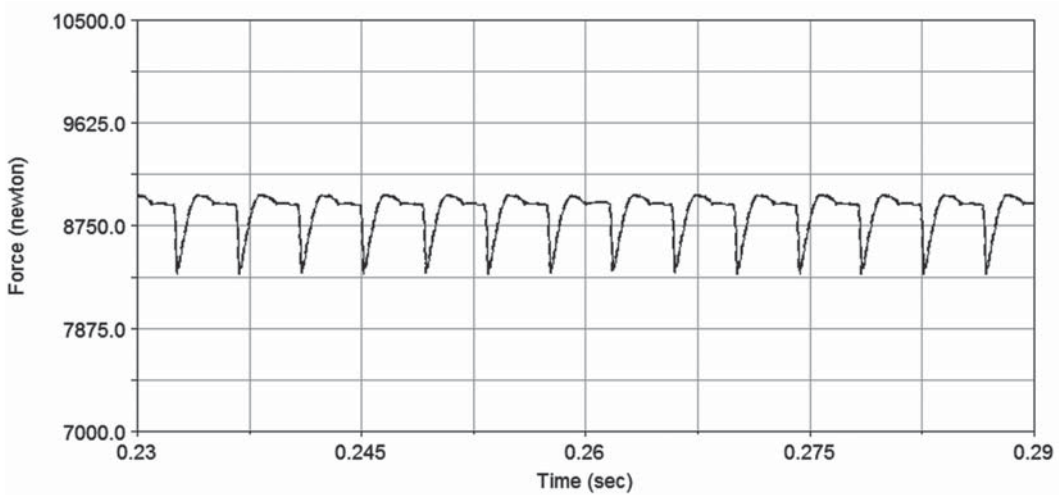

Fig. 3. Meshing force

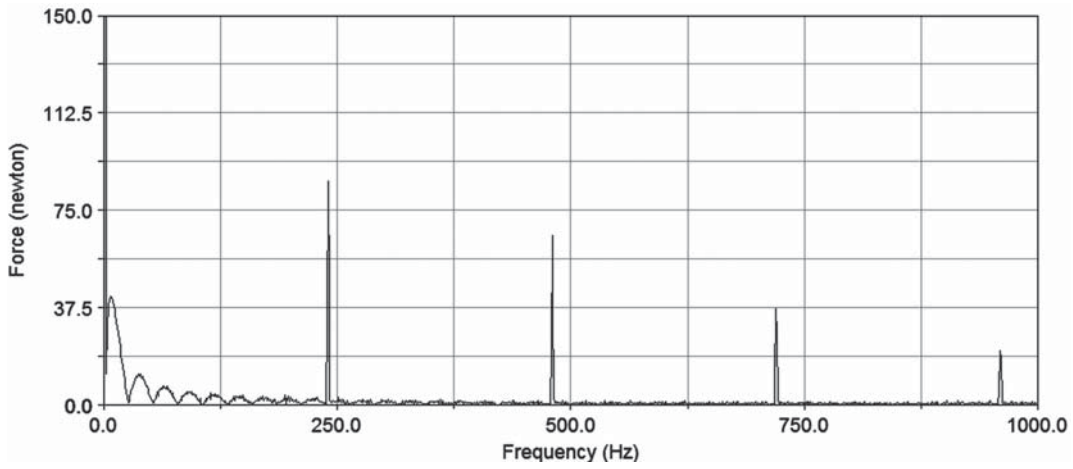

Fig. 4. Spectrum of meshing force

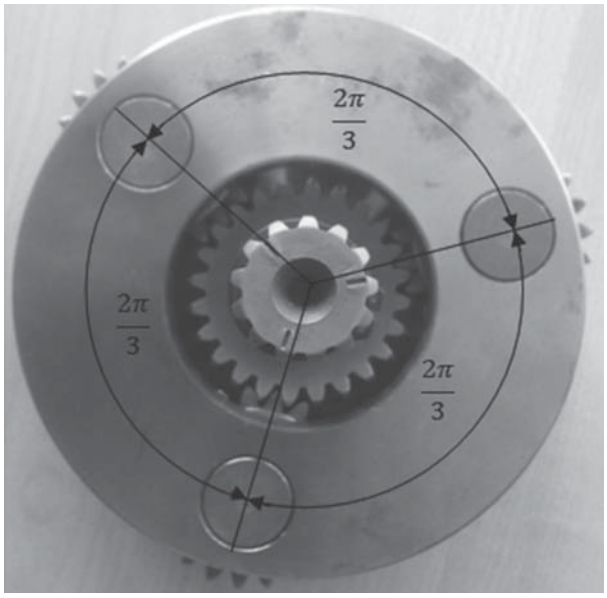

Fig. 5. Planetary gear MERCURY 1-A

To build the model next assumptions were done: gears and shafts are rigid, contact surfaces are elastic, ideal teeth profile, gears are made from steel without surface treatment, lubrication neglected. Firstly the CAD model was developed, next it was imported to the ADAMS environment. In the multi-body dynamics software the constraints and forces were modeled. The three-dimensional CAD model of the planetary gear is presented in Figure 6.

To conduct dynamic simulations of the model, forces and torques were defined. In the model the torque of 60 Nm was applied on the carrier and constant rotational speed of 30 Hz was applied on the shaft of the sun gear. To verify the model, firstly displacements of the mass centers of the planet gears in the global coordinates system, during simulation was presented, Figure 7.

On the plots above the phase relations between the positions of each gear resulting from the geometric properties are visible. In the next chapter the analysis of vibration signals generated by the model were presented.

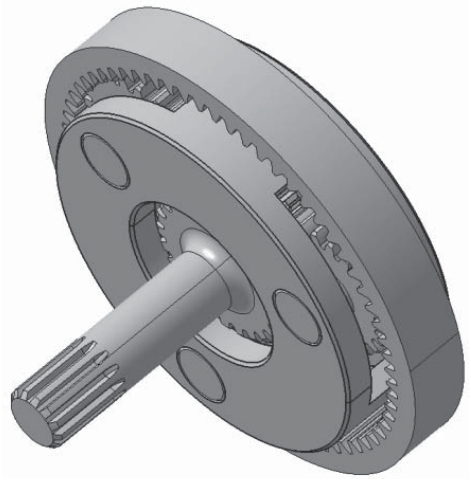

Fig. 6. Planetary gear CAD model

4. SIMULATION RESULTS

In this chapter the model simulations results were presented. The simulations were conducted for the same parameters and operations as presented in the previous chapter. In the study the meshing force signal was measured in the vertical direction in global coordinates during tests. The analysis of the tests results were presented in Figure 8 and 9.

The changes of the contact force between the planet and ring gear are presented in Figure 8, while in Figure 9 the spectral analysis of this signal was presented. On the spectrum characteristic frequencies of the planetary gear system are observable. The frequency of 8 Hz is related to the carrier rotations f_a, equation (7).

$$f_a = f_1 \frac{z_1}{z_1 + z_2} = f_1 \cdot 0.266. \tag{7}$$

In the equation above $z_1 = 24$ is a teeth number of sun gear, $z_3 = 66$ is a the teeth number of ring gear and $f_1 = 30$ Hz is a the rotational speed of the input shaft.

$$f_{12} = f_{23} = f_1 \frac{z_1 z_2}{z_1 + z_2} = f_1 \cdot 17.6 \tag{8}$$

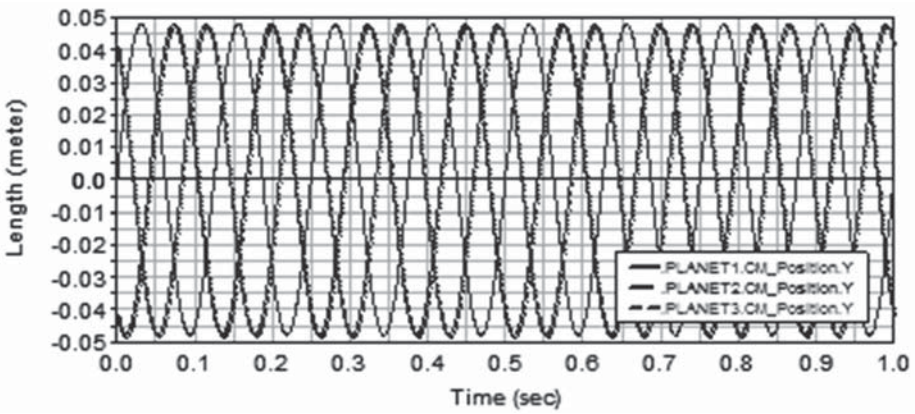

Fig. 7. Planet gear center mass position during simulation

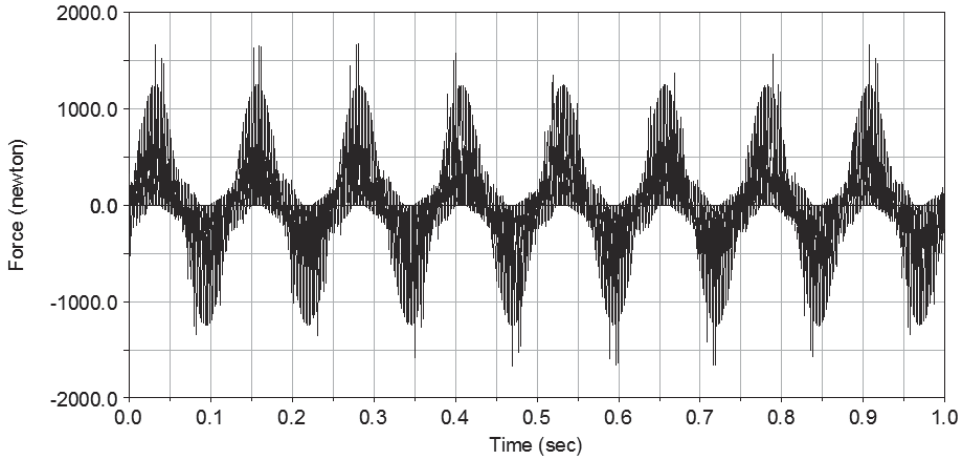

Fig. 8. Meshing force generated by planet and ring gear

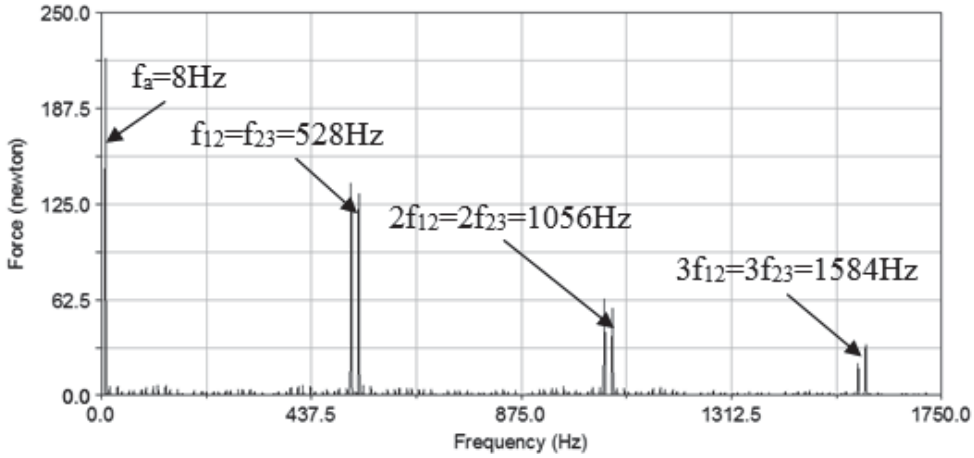

Fig. 9. Spectral analysis of meshing force generated by planet and ring gear

The planetary gear meshing frequency harmonics are presented by the equation (8), the first three harmonics should be localized on 528, 1056 and 1584 Hz. On the spectrum one can observe that the GMFs were reduced, only modulations of this frequencies by carrier rotation speed are visible. The reduction can be caused by ideal geometry of the planetary gear system. The meshing forces generated by three planet gears were plotted in Figure 10.

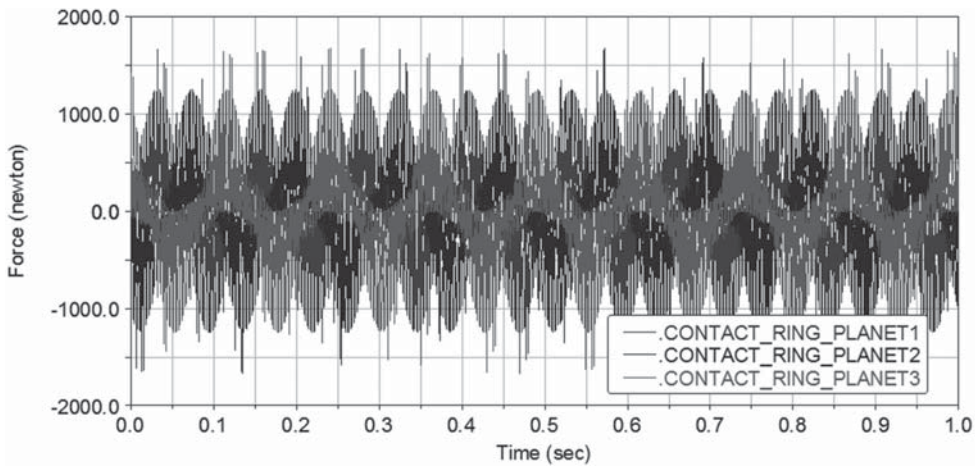

Fig. 10. Meshing forces generated by three planet gears and ring gear

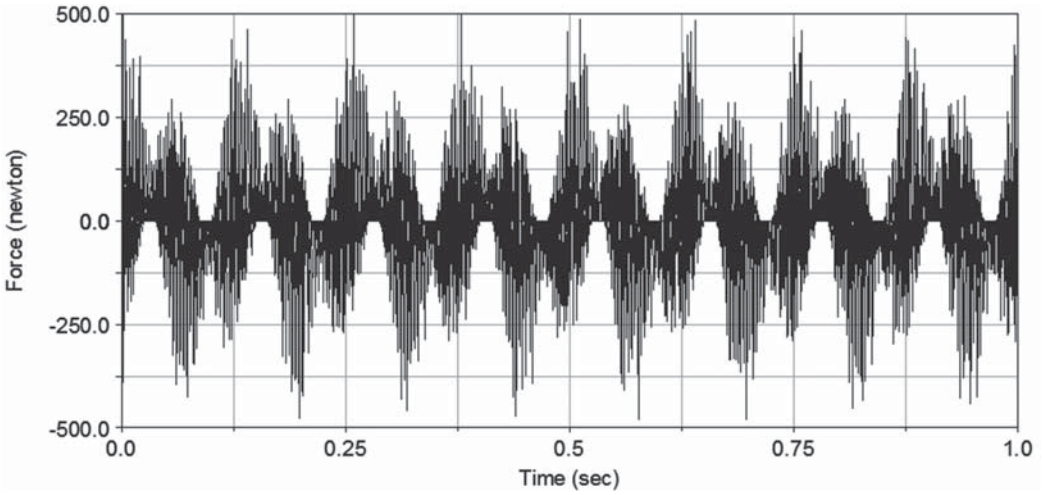

Fig. 11. Meshing force generated by planet and sun gear

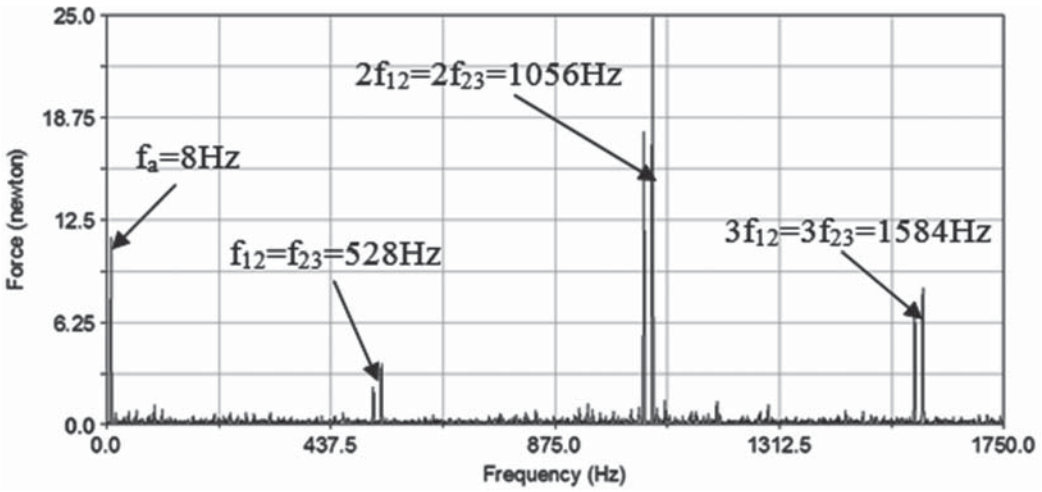

Fig. 12. Spectral analysis of meshing force generated by planet and sun gear

The meshing forces generated by the planet and ring gear were plotted in figure above. The phase shift between these signals is clearly observable.

In the next part of this chapter analogous analysis for the signals generated by the sun and planet gears were presented.

As it is observable in Figure 11 for this case the changes of the force signal are similar as for the planet-ring gear meshing. The periodical changes of the force sign are due the position changes of the planet gears during operations in the global coordinate system. On the spectrum presented in Figure 12, it is visible that for this case the even modulations have signify bigger amplitudes.

5. CONCLUSIONS

In the presented paper the tests results of the planetary gear dynamic model were presented. In the conducted simulations the vibration signals were generated by the contact algorithm, acting during interactions between gears teeth. On the spectra of meshing force the harmonics of carrier and gear meshing frequencies harmonics are observable. The localization of the gear meshing frequency harmonics is correct for assumed operation conditions. It can be concluded that in the presented model contact forces between the sun and planetary gears are three times smaller, than generated by ring and planet gear meshing process. In the paper the preliminary tests of the multi-body model of planetary gear were presented. In the future the model will be extended, e.g. by application of flexible bodies for gears and shafts, taking into account lubrication, analysis of signals propagation paths from meshing points to sensor located on the gearbox housing.

This study was supported by Grant No. 15.11.130.146

References

Dresig H., Schreiber U. 2005, *Vibration Analysis for Planetary Gears*, Proc. of the International Conference on Mechanical Engineering and Mechanics, Nanjing, China.

Johnson K. L. 1985, *Contact Mechanics*, Cambridge University Press.

Kong D., Meagher J. M., Xu C., Wu X., Wu Y. 2008, *Nonlinear Contact Analysis of Gear Teeth for Malfunction Diagnostics*, Proc. of the IMAC XXVI Conference and Exposition on Structural Dynamics, Orlando, Florida.

Sommer A., Meagher J., Wu X. 2011, *Gear Defect Modeling of a Multiple-Stage Gear Train*, Modeling and Simulation in Engineering, vol. 2011, pp. 1–8.

Wojtyra M., Frączek J. 2007, *Metoda układów wieloczłonowych w dynamice mechanizmów*, Oficyna Wydawnicza Politechniki Warszawskiej.

Wu X., Meagher J., Sommer A. 2011, *A Differential Planetary Gear Model with Backlash and Teeth Damage*, Rotating Machinery, Structural Health Monitoring, Shock and Vibration, no. 5, pp. 203-215.

MSC Inc. 2011, MSC ADAMS reference manual.

MECHANICS AND CONTROL
Vol. 31 No. 4 2012 http://dx.doi.org/10.7494/mech.2012.31.4.158

Janusz Piechowicz*, Paweł Pawlik*

MULTICHANNEL DATA ACQUISITION SYSTEM FOR VIBROACOUSTIC SIGNALS

SUMMARY

The authors have made an attempt to construct a multi-channel data acquisition system for vibroacoustic signals, collected for analysis of acoustic field distributions in enclosed rooms and determination of surface acoustic impedance values at the wall surfaces. The scope of the study required a synchronic registration of acoustic pressure by 24 measurement microphones, determination of the phase-shift angles between the measured signals and determination of the vibration velocity for the loudspeaker diaphragm. The paper presents the first stage of the research, directly related to the multi-channel system for registration and analysis of vibroacoustic signals. The constructed research tools, due to their modular structure, can be adapted to new tasks, extended by adding new elements (further measurement cards, microphones, accelerometers etc.), what ensures great flexibility and suitability of the system for realization of advanced acoustical measurements. Open source code and users request for specialized acoustic analyses make the developed software packages a highly prospective research tool both for today and tomorrow.

Keywords*: measurement systems, acoustic impedance, synchronous measurement, acoustic measurements*

WIELOKANAŁOWY SYSTEM AKWIZYCJI SYGNAŁÓW WIBROAKUSTYCZNYCH

Autorzy podjęli zadanie budowy wielokanałowego systemu akwizycji sygnałów wibroakustycznych na potrzeby analizy rozkładów pola akustycznego w pomieszczeniach i wyznaczania wartości impedancji akustycznej powierzchni ścian. Program badań wymagał synchronicznej rejestracji ciśnienia akustycznego przez 24 mikrofony pomiarowe, wyznaczenia kąta przesunięcia fazowego między mierzonymi sygnałami oraz wyznaczenia amplitudy prędkości drgań membrany głośnika. W pracy przedstawiony jest pierwszy etap badań bezpośrednio związany z wielokanałowym systemem rejestracji i analizy sygnałów wibroakustycznych. Zbudowano narzędzia, które dzięki modułowej strukturze mogą być dostosowywane do nowych zadań, rozszerzane o nowe elementy (kolejne karty pomiarowe, mikrofony, akcelerometry itp.), co stanowi o dużej przydatności powstałego systemu do zaawansowanych pomiarów akustycznych. Otwarty kod źródłowy oraz autorskie zapotrzebowanie na specjalistyczne analizy akustyczne tworzą z opracowanych pakietów programowych w pełni rozwojowe narzędzie badawcze na dziś i na przyszłość.

Słowa kluczowe*: systemy pomiarowe, impedancja akustyczna, pomiar synchroniczny, pomiary akustyczne*

1. INTRODUCTION

In many research and diagnostic problems in vibroacoustics one encounters tasks related to synchronic acquisition of big volumes of measurement data, acquired from parameter distributions of acoustic field surrounding the examined objects or located inside the objects. Such tasks are usually carried out in the first stage of vibroacoustic signal analysis, preparing the data for further processing or interpretation. The basis for construction of a system capable of executing such a task is the proper formulation of the research objectives and arrangement of a proper hardware measurement system. The data acquisition usually comprises a sequence of steps:

– Defining the measured quantities.
– Acquisition of signals from the sensors.
– Transmission to the recording device.
– Time sampling.
– Value quantization.
– Signal processing for the analysis requirements.

The authors have made an attempt to construct a multi-channel data acquisition system for vibroacoustic signals, collected for analysis of acoustic field distributions in enclosed rooms and determination of surface acoustic impedance values at the wall surfaces (Piechowicz et al. 2011). The proposed research methodology required completion of several stages consisting of preparatory tasks:

1. Construction of a model measurement test stand – selection of equipment, positioning of the measuring microphones, specification of the measured quantities.
2. Elaboration of a dedicated software package for acquisition of the measured data.
3. Elaboration of the software used for analysis and processing of the data collected from the measurements.
4. Construction of the 3D computer model for the examined room.
5. Development of specialized software for calculation of the surface impedance of bounding walls, using the inverse boundary element method.

* AGH University of Science and Technology, Department of Mechanics and Vibroacoustics, Krakow, Poland; piechowi@agh.edu.pl

Because of new, nonstandard procedures introduced to the problem solution the scope of the research activity has been divided into two parts:

– Studies of the model room.
– Studies carried out in the real-world room.

In the first part of the study the required measurement quantities have been defined (the averaged amplitudes of acoustic pressure, phase-shift angles between the individual acoustic signals registered in the measurement, vibration velocity for the sound source diaphragm). Then the additional requirements have been formulated, regarding the configuration of the measurement setup, positioning of the measuring microphones and software used for measuring, recording and analysis of measured signals. Functioning of the whole system has been tested and verified by carrying measurements in a specially made model room.

The second part of the study comprised a construction of numerical models of the examined objects, elaboration of software for simulation of acoustic field distributions, analysis of the results and introducing corrections if necessary (Piechowicz 2011).

The paper presents the first stage of the research, directly related to the multi-channel system for registration and analysis of vibroacoustic signals.

2. CONFIGURATION OF THE MEASUREMENT CIRCUIT

The scope of the study required a synchronic registration of acoustic pressure by 24 measurement microphones, determination of the phase-shift angles between the measured signals and determination of the vibration velocity for the loudspeaker diaphragm. The measurement setup also included a generator of sinusoidal and noise signals for stimulation of the enclosed space volume (model room or the real-world room under examination). For the measurements of the sound field parameters a dedicated multi-channel data acquisition system has been constructed, based on the PXI hardware platform. The system included NI PXI-1042Q type chassis, NI PXI-8196 controller (see Fig.1) and the following measurement cards:

– *three measurement cards type NI PXI-4472B with the following basic features:*
  • *eight simultaneously sampled vibration-optimized analog inputs,*
  • *maximum sampling rate102.4 kS/s,*
  • *measurement range ± 10 V, 24 bit resolution;*
– *one NI PXI-4461 measurement card:*
  • *two simultaneously sampled analog inputs:*
  • *maximum sampling rate 204.8 kS/s,*
  • *two simultaneously updated analog outputs:*
  • *maximum sampling rate 204.8 kS/s,*
  • *maximum measurement range ± 42.4 V; 24 bit resolution.*

Registration of the measured signals has been carried out by:

– *24 professional ¼" matrix microphones,*
– *laser vibrometer.*

The measurement setup included also:

– *amplifier,*
– *loudspeaker,*
– *the elements positioning the measurement microphones.*

The measurement circuit has been calibrated both in amplitude and phase-shift angle using an acoustic calibrator with a specialized 6-way attachment, allowing simultaneous calibration of six ¼" microphones. The analog output of the NI PXI-4461 card has been used for generation of the tonal signal stimulating the boundary elements of model room or the real-world object, and the 25-th measurement channel (one of the two analog input channels of the NI PXI-4461 card) has been used for registration of the laser vibrometer signal, the device dedicated to the measurements of the vibrating surface (loudspeaker diaphragm) displacement, using the interference effects.

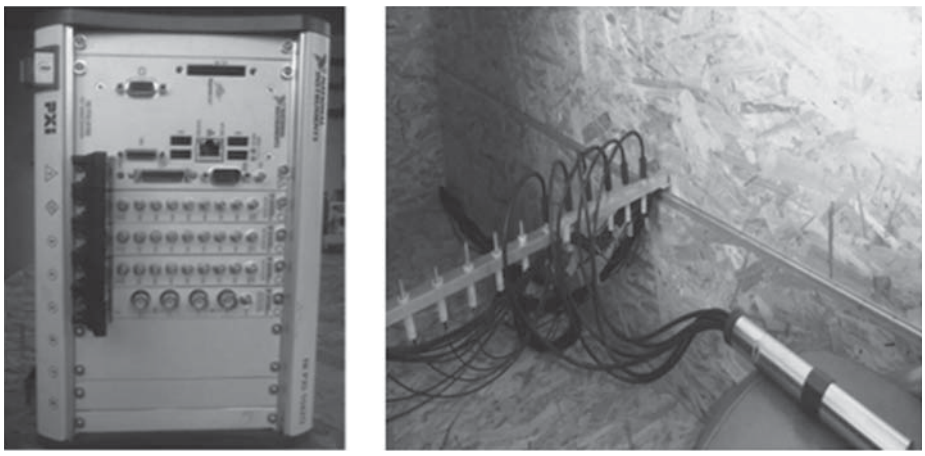

Fig. 1. The NI PXI 1042Q chassis with three NI PXI 4472B cards and one NI PXI-4461 card (a), The model room with a line of microphones (b)

The PXI (PCI eXtension for Instrumentation) platform includes the PXI Trigger Bus, what allows full measurement synchronization between individual modules. PXI makes use of all advantages offered by the standard software and hardware PCI architecture, including fast data transfer. The fast PCI bus, used by the PXI, when combined with integrated clock rate signal and triggering, allows a convenient implementation of PXI devices to synchronic, multi-channel measurements. In short the PXI is a modular platform for measuring devices, which allows realization of various measurement functions controlled by the supervising PC.

3. THE MEASUREMENT SOFTWARE

For realization of the acoustic measurements and processing of the measured data two dedicated software packages have been developed by the authors:

– *Multichannel Data Acquisition System,*
– *Spectral Analyzer.*

Both software packages have been written in the LabView 2010 environment. The LabVIEW environment includes advanced numerical libraries and the necessary drivers enabling the cooperation with various external devices. The DAQmx drivers enable access to all the modules of the PXI platform, what allows the hardware configuration according to the user's own needs. The applications allowed the creation of virtual measurement devices for specialized measurements, using multi-channel signal registration, and for the later signal analysis. During the measurement process the acoustic signals are registered on the hard disk in the lossless TDMS standard. The lossless registration of the time dependencies allows convenient re-analysis of the data after each software modification.

The constructed tools, due to their modular structure, can be adapted to new tasks, extended by introducing new elements (additional measurement cards, microphones, accelerometers etc), what ensures the systems suitability for performing new, more advances acoustic measurements.

3.1. Multichannel Data Acquisition System

The multithreading architecture of the *Multi-Channel Data Acquisition System* (see Fig. 2) is dedicated to synchronic acquisition of signals from multiple channels (26 measurement channels), which is synchronized with the measurements of generation parameters of tonal or noise signals (2 channels). This type of architecture, has also been used in (Batko et al. 2012).

In the acquisition thread the measurement process has been configured in such a way that individual signals, measured and generated by various measurement cards, are fully synchronized. The signal acquisition has been synchronized with the voltage signal generating the acoustic stimulation using the loudspeaker, so that the phase-shift angles between the individual registered signals can be easily analyzed.

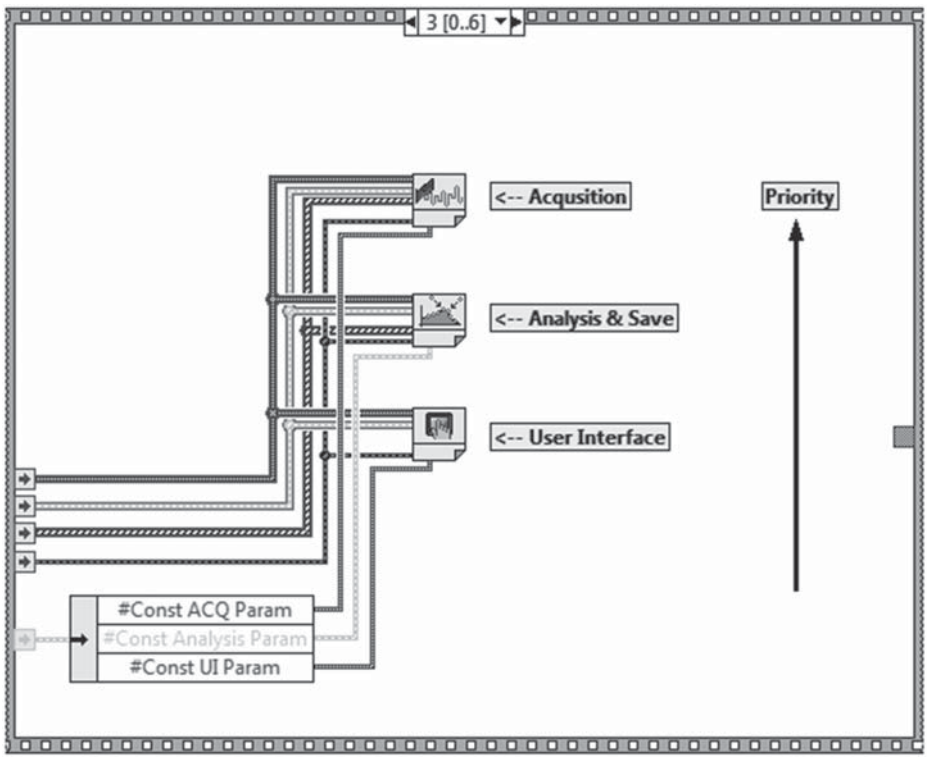

Fig. 2. Structure of the *Multi-channel Data Acquisition System* application, developed in the LabVIEW environment

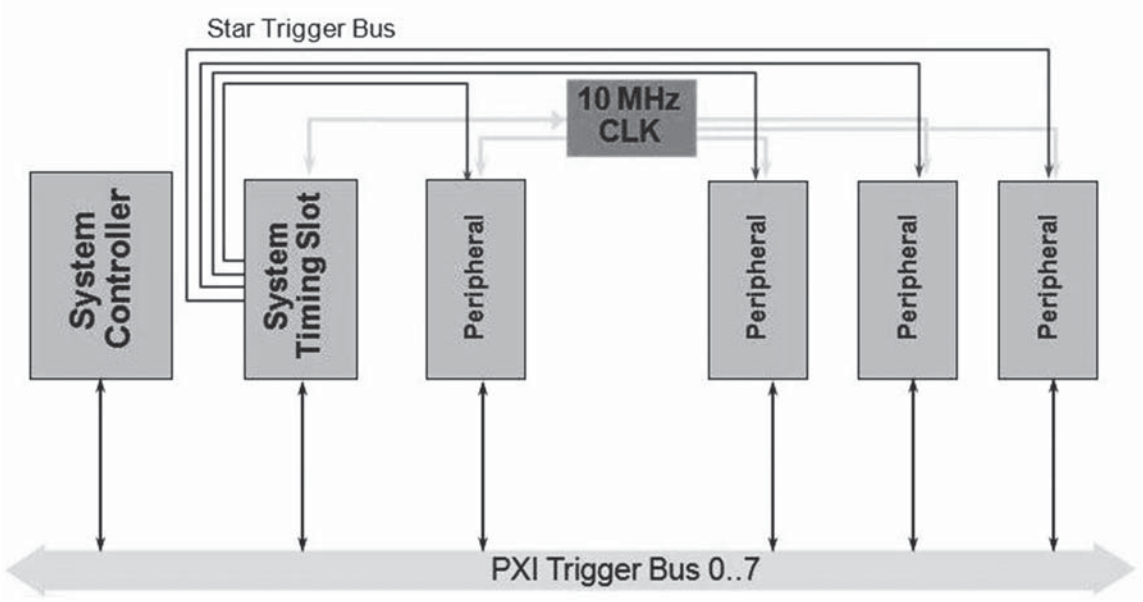

Fig. 3. Block scheme of synchronization lines connection in the PXI platform (National Instruments 2007)

Measurement triggering is executed using the PXI Trigger Bus (Fig. 3), which enables simultaneous measurement triggering for all the measuring cards. The maximal delay on the PXI Trigger Bus is estimated to be about 80 ns. In addition all the measurement cards execute the sampling of analog signals using the Sample Clock, located in the NI PXI-4472B card, installed in the System Timing Slot.

The acquisition thread works with the highest priority, in order to ensure the lossless acquisition of the measured data. The collected data are sent to data analysis thread, using the FIFO queue.

The next thread executes the preliminary data processing for the purpose of later data presentation on the user's interface panel. That module also includes the calibration of the measurement system and the recording of measurement data.

The duration of the calibration are 5 seconds, during which time the average value is calculated for each microphone sensitivity sen_{mean} (1) and the phase shift relative to the first microphone φ_{mean} (2), at a given signal from the calibrator standard six-pin special adapter (Fig.1).

$$sen_{mean} = \frac{1}{n}\sum_{i=1}^{n} sen_i \tag{1}$$

$$\varphi_{mean} = \frac{1}{n}\sum_{i=1}^{n} \varphi_i \tag{2}$$

where:

n – number of measurement windows;

sen_i – microphone sensitivity determined in a single measurement window [mV/Pa];

φ_i – phase shift relative to the first microphone set in a single measurement window [rad].

In the whole structure the supervision and control of individual threads is executed by the *User Interface* thread, which sends the proper commands to the other threads and deals with the messages concerning possible errors. It is also responsible for the communication between the user and the program (modification of the registration parameters, presentation of the results).

During the measurement the monitor screen presents the time dependencies and power spectra registered from individual measurement channels and simultaneous preview of acoustic pressure RMS values for all the measurement channels. Figure 4 presents the main window of the *Multi-channel Data Acquisition System* application.

The application also realizes the generation of sinusoidal signal of a specified frequency and amplitude. Additionally a Gaussian noise signal of required amplitude can be also generated.

3.2. Spectral Analyzer

The collected and written to TDMS type disc file measurement data are analyzed using the analysis application called *Spectral Analyzer*. The application is compatible with the *Multi-channel Data Acquisition System* described above. In the application band analysis functions for a selected signal have been implemented for frequency bands of 1/24, 1/12 and 1/3 octave width as well as full octave analysis. The frequency band analysis is carried out with specified additional parameters like: bandwidth, correction curve type (A, B, C and linear), averaging method and the range of the analyzed frequency band. Additionally the user can carry out the spectral analysis in a single frequency band of a selected range and calculate the amplitude-frequency and phase angle-frequency characteristics of tested objects.

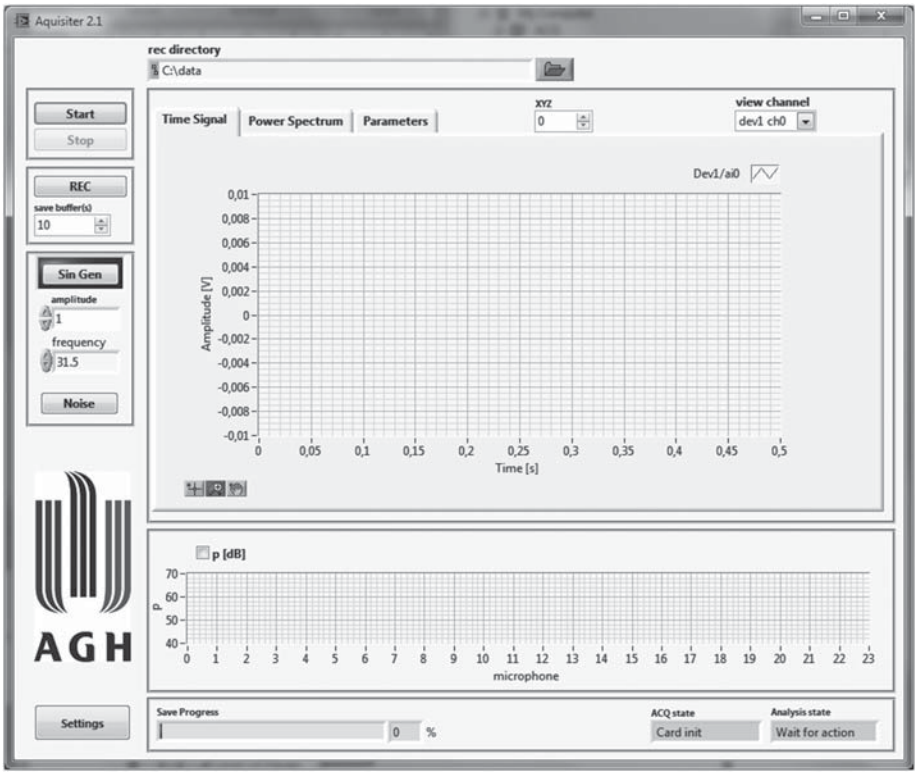

Fig. 4. The main window of the *Multi-channel Data Acquisition System*

The *Spectral Analyzer* application, dedicated to analysis of written time signals, includes also the function of automated analysis of all the data written in TDMS type files (see Fig. 5 and Fig. 6). The application automatically executes the amplitude-frequency analysis and phase angle analysis for the signals measured with Gaussian noise stimulation for the selected measurement channel. If the signal has been measured with sinusoidal stimulation it calculated the phase-shift angle between the diaphragm velocity measurement signal (for the loudspeaker emitting the stimulation signal) and the signals registered by the individual measurement microphones. It also calculates the RMS values for signals registered by individual microphones and for the channel registering the loudspeaker diaphragm vibration velocity.

The results of the analyses are written to two TXT files. One of the files contains the results of analysis for signals measured with sinusoidal stimulation, while the results of analyses for signals measured with the noise type stimulation are written to the other (separate) file.

Fig. 5. The *Spectral Analyzer* application, *Octave Spectrum* Tab

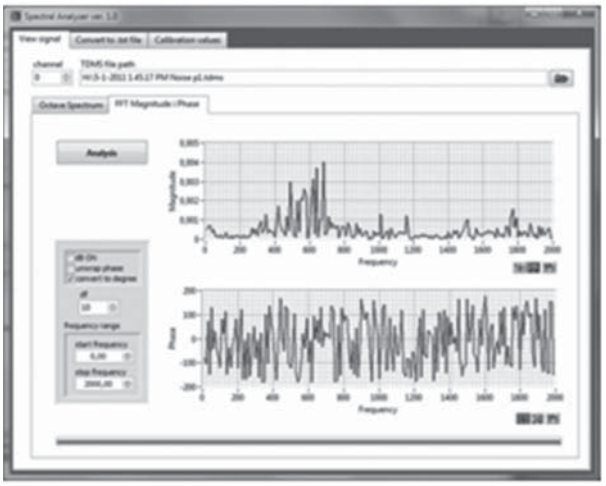

Fig. 6. The *Spectral Analyzer* application, *FFT Magnitude and Phase* Tab

4. SUMMARY

Multi-channel system for acquisition of vibroacoustic signals has been constructed for realization of a specific research program. Its structure and accompanying software allow its further development by multiplying the number of measurement channels, realized by the possibility to add further measurement cards and to connect further sensors. The dedicated software, written in the LabVIEW environment, allows creation of virtual measurement devices for specialized, multi-channel data acquisition of vibroacoustic signals and spectral analysis. The measured data are written as time-dependent sound pressure values, what allows repeated analyses after each modification of the analyzing procedure. The TDMS data recording standard in addition to time-dependent functions allows also appending description notes for the recorded signals as well as measurement parameters.

The constructed research tools, due to their modular structure, can be adapted to new tasks, extended by adding new elements (further measurement cards, microphones, accelerometers etc.), what ensures great flexibility and suitability of the system for realization of advanced acoustical measurements. Open source code and users request for specialized acoustic analyses make the developed software packages a highly prospective research tool both for today and tomorrow.

This paper was carried out in the part of the activities statutory Department of Mechanics and Vibroacoustics AGH UST in Cracow.

References

National Instruments 2007, *Synchronization Explained*, http://www.ni.com/.

Batko W., Korbiel T. Pawlik P. 2012, *Analiza eksperymentalna przydatności trajektorii fazowych do diagnostyki maszyn wirujących*, Problemy Eksploatacji – Maintenance Problems, No. 1, pp. 7–15.

Piechowicz J. et al. 2011: *Sprawozdanie z realizacji projektu badawczego N N504 342536 Zastosowanie metody inwersji w analizie własności akustycznych pomieszczeń przemysłowych*, AGH Kraków, (maszynopis)

Piechowicz J. 2011, *Estimating surface acoustic impedance with the inverse method*, International Journal of Occupational Safety and Ergonomics, **17**, 3, pp. 271–276.